

Stellar Inversion Techniques

Daniel R. Reese

Abstract Stellar seismic inversions have proved to be a powerful technique for probing the internal structure of stars, and paving the way for a better understanding of the underlying physics by revealing some of the shortcomings in current stellar models. In this lecture, we provide an introduction to this topic by explaining kernel-based inversion techniques. Specifically, we explain how various kernels are obtained from the pulsation equations, and describe inversion techniques such as the Regularised Least-Squares (RLS) and Optimally Localised Averages (OLA) methods.

1 Introduction

Many of the problems which intervene in physics can be described in terms of forward and inverse problems. Generally speaking, a forward problem focuses on predicting the effects which result from a set of physical causes, such as deducing the gravitational field of an object from its distribution of matter. In an inverse problem, one typically tries to deduce the physical causes which led to a given set of results or effects (which are typically observations). Hence, trying to deduce the distribution of matter from the gravitational field of an object is an inverse problem.

The field of asteroseismology, i.e., the study of stellar pulsations, also fits this description. Trying to predict stellar pulsation frequencies for a given stellar model constitutes a forward problem. Likewise, trying to deduce the stellar structure which led to a given set of pulsation frequencies is an inverse problem. This inverse problem turns out to be quite difficult because, in general, the relation between stellar structure and oscillation frequencies is non-linear. Nonetheless, given the wealth of

Daniel R. Reese
LESIA, Observatoire de Paris, PSL Research University, CNRS, Sorbonne Universités, UPMC
Univ. Paris 06, Univ. Paris Diderot, Sorbonne Paris Cité, 92195 Meudon, France,
e-mail: daniel.reese@obspm.fr

information on the internal structure of stars provided by pulsation frequencies, a variety of approaches have been devised to tackle this problem, as expressed by Gough (1985) in the context of helioseismology:

Inversions can conveniently be divided into three categories. The simplest consists of the execution of the forward problem using solar models with a few adjustable parameters, and the calibration of those parameters by fitting theory to observation. The second is the use of analytical methods. [...] Thirdly, there are the formal inversion techniques borrowed from geophysics that have been used on real and artificial solar data.

The first category of inversions is usually named “forward modelling” (not to be confused with the “forward problem”) and corresponds to searching for an optimal model in a restricted parameter space. It typically includes methods such as grid searches (e.g., Silva Aguirre et al. 2015), MCMC methods (e.g., Bazot et al. 2012), or genetic algorithms (Metcalf & Charbonneau 2003, Charpinet et al. 2005). The advantages of this approach is its obvious simplicity, and the fact that it produces physically coherent models. However, the parameter space is restricted and does not allow for hitherto unknown physical ingredients not included in the stellar models. Furthermore, such methods can be costly, especially if models are calculated on-the-fly. The second approach includes methods such as asymptotic methods or glitch fitting. These methods can provide a great deal of physical insight into stellar physics but are beyond the scope of the present lecture. Finally, formal inversion techniques typically consist in adjusting the structure of a reference stellar model so as to match a set of observed frequencies. The advantage of this approach is that it can potentially extract more information from the pulsation frequencies, and is therefore open to new physics. However, this method may lead to models which are not physically coherent, and can be more difficult to implement. These approaches are in fact complementary. Indeed, the forward approach typically provides a reference model, which can then be further refined via formal inversion techniques.

The present lecture focuses on the third category, i.e., formal inversion techniques. However, before tackling inversions, it is necessary to spend a bit of time on the forward problem in order to bring out some of the properties which apply in the context of inverse problems. This will be the subject of the next section. Then stellar inversion techniques will be described in Sect. 3. A short conclusion including a list of relevant references and available inversion codes will follow.

2 The forward problem

2.1 Adiabatic pulsation equations

Stellar pulsations, the periodic motion of gas or plasma within a star, are described by the Lagrangian displacement and the Eulerian perturbations to density, pressure, and gravitational potential, denoted ξ , ρ' , p' and ϕ' , respectively. When applying the adiabatic approximation (i.e., when neglecting heat transfers during the peri-

odic motions), these quantities are determined by Euler’s equation, the continuity equation, and the adiabatic relation, which express the conservation of momentum, mass, and energy, as well as Poisson’s equation. Through various analytical manipulations, and the use of Green’s function and suitable boundary conditions for Poisson’s equation, it is possible to express ρ' , p' and ϕ' as a function of ξ alone. When inserted into Euler’s equation, this leads to the following schematic equation:

$$\omega^2 \xi = \mathcal{F}(\xi), \quad (1)$$

where \mathcal{F} is an integro-differential operator, and where we have assumed a time dependence¹ of the form $\exp(-i\omega t)$. Equation (1), along with appropriate boundary conditions, is an eigenvalue problem, the solutions of which are known as “eigen-solutions”. Specifically, ω^2 is an eigenvalue and corresponds to the square of the pulsation frequency, whereas ξ is the eigenmode or eigenfunction, and specifies the geometric characteristics of the stellar pulsation.

The forward problem in this case, then corresponds to finding the above eigen-solutions for a given stellar structure, i.e., for a given \mathcal{F} operator. The inverse problem corresponds to finding the stellar structure (and hence \mathcal{F}) from a set of pulsation frequencies and some sort of mode identification, i.e., a partial characterisation of the structure of the pulsation modes. In the case of solar-like oscillators, a mode identification typically includes the harmonic degrees ℓ of the pulsations, and possibly the radial orders n (this is usually obtained from comparisons with models) and azimuthal orders m (only if frequency multiplets, typically caused by stellar rotation, can be resolved). Given that the forward problem is non-linear, the inverse problem will also be non-linear. However, to make the problem more tractable, one typically linearises it. Linearising Eq. (1) leads to the following equation²:

$$(\delta\omega^2)\xi + \omega^2(\delta\xi) = \delta\mathcal{F}(\xi) + \mathcal{F}(\delta\xi). \quad (2)$$

This equation simply expresses how a small modification to the stellar structure leads to small modifications³ of the pulsation modes, in particular frequency differences $\delta\omega$. Hence, in order to solve the inverse problem, one needs to find a reference stellar model (typically using some form of forward modelling) which is sufficiently close to the true stellar model so that the linear approximation applies, and *invert* the frequency differences, in order to find how to correct the stellar model so that it more closely matches the actual star. However, Eq. (2) is not straightforward to use as it contains terms with $\delta\xi$, the perturbation of the eigenmode. The next section shows how to remove these terms by exploiting an important property of the adiabatic pulsation equations, namely their symmetry.

¹ If one assumes that modes are proportional to $\exp(im\varphi)$, φ being the longitude, such a time dependence will lead to $m > 0$ modes being prograde, where m is the azimuthal order. If one uses, instead, a time dependence of the form $\exp(i\omega t)$, then $m > 0$ modes will be retrograde.

² Throughout these lectures, the δ notation will be used to indicate a modification of the equilibrium stellar structure and associated pulsations.

³ It is very important to note that here, the “ δ ” symbol is not a Lagrangian perturbation, but rather a modification of the model and its pulsations.

2.2 Symmetry of the adiabatic pulsation equations

Before explaining in what sense the pulsation equations are symmetric, it is necessary to introduce the following dot product:

$$\langle \boldsymbol{\eta}, \boldsymbol{\xi} \rangle = \int_V \rho_0 \boldsymbol{\eta}^* \cdot \boldsymbol{\xi} dV, \quad (3)$$

where $\boldsymbol{\eta}^*$ is the complex conjugate of $\boldsymbol{\eta}$, and V the stellar volume. We note that this is a complex dot product, hence: $\langle \boldsymbol{\eta}, \boldsymbol{\xi} \rangle = \langle \boldsymbol{\xi}, \boldsymbol{\eta} \rangle^*$.

The adiabatic pulsation equations are symmetric with respect to the above dot product:

$$\langle \boldsymbol{\eta}, \mathcal{F}(\boldsymbol{\xi}) \rangle = \langle \mathcal{F}(\boldsymbol{\eta}), \boldsymbol{\xi} \rangle, \quad (4)$$

where $\boldsymbol{\xi}$ and $\boldsymbol{\eta}$ are any displacement fields, which need not necessarily be eigenfunctions at this point. In order to prove this symmetry, we start by introducing the associated pressure and gravitational potential perturbations as deduced from the relevant equations: $(\boldsymbol{\xi}, p', \phi')$ and $(\boldsymbol{\eta}, \pi', \psi')$. We then calculate the dot product between $\boldsymbol{\eta}$ and Euler's equation (applied to $\boldsymbol{\xi}$). After various manipulations (integration by parts etc.), this leads to the following formula (e.g., Unno et al. 1989):

$$\begin{aligned} \langle \boldsymbol{\eta}, \mathcal{F}(\boldsymbol{\xi}) \rangle &= \int_V \frac{(\pi')^* p'}{\rho_0 c_0^2} dV + \int_V \rho_0 N_0^2 (\boldsymbol{\eta}^* \cdot \mathbf{e}_r) (\boldsymbol{\xi} \cdot \mathbf{e}_r) dV \\ &+ \int_S \rho_0 g_0 (\boldsymbol{\eta}^* \cdot \mathbf{e}_r) (\boldsymbol{\xi} \cdot \mathbf{e}_r) dS - \frac{1}{4\pi G} \int_{V_\infty} \nabla(\psi')^* \cdot \nabla \phi' dV, \end{aligned} \quad (5)$$

where V is the star's volume, S its surface, V_∞ infinite space, \mathbf{e}_r the unit vector in the radial direction, and N_0^2 the square of the Brunt–Väisälä frequency. In deriving the surface term, we assumed, as a boundary condition, that the Lagrangian pressure perturbation vanishes at the surface. Appendix C of Reese (2006) explains how to obtain the last term (integrated over V_∞). It is very clear from this explicit formulation that the pulsation equations are symmetric. More general forms of this equation have been derived, for instance, in the case of differentially rotating physical bodies (Lynden-Bell & Ostriker 1967).

This symmetry leads to a number of consequences. Firstly, the eigenvalues, ω^2 , are real (meaning that the ω are either real or purely imaginary). Secondly, the eigenfunctions of distinct eigenvalues are orthogonal with respect to the above dot product. The third consequence is known as the ‘‘variational principle’’. According to this principle, the variational frequency, defined by $\omega_{\text{var}}^2 = \langle \boldsymbol{\xi}, \mathcal{F}(\boldsymbol{\xi}) \rangle / \langle \boldsymbol{\xi}, \boldsymbol{\xi} \rangle$, differs from the true eigenfrequency by an amount which is of second order or higher in terms of the error on the eigenfunction, i.e., $\omega^2 - \omega_{\text{var}}^2 = \mathcal{O}(\|\Delta \boldsymbol{\xi}\|^2)$. This is useful as ω_{var}^2 provides an independent and potentially more accurate estimate of the eigenvalue than the numerical value and is therefore used as an accuracy test in various pulsation codes such as ADIPLS (Christensen-Dalsgaard 2008).

2.3 Kernels

We now return to our original problem, i.e., calculating the frequency variation caused by a small modification of the stellar structure. Taking the dot product between Eq. (2) and ξ , and grouping terms with $\delta\xi$ yields:

$$\delta\omega^2 \langle \xi, \xi \rangle - \langle \xi, \delta\mathcal{F}(\xi) \rangle = \langle -\omega^2 \xi + \mathcal{F}(\xi), \delta\xi \rangle, \quad (6)$$

where we have made use of the symmetry of \mathcal{F} . The right-hand side vanishes because ξ is an eigenmode, and ω^2 the corresponding eigenvalue. Isolating $\delta\omega^2$ then yields:

$$\delta\omega^2 = 2\omega\delta\omega = \frac{\langle \xi, \delta\mathcal{F}(\xi) \rangle}{\langle \xi, \xi \rangle}. \quad (7)$$

This last form is extremely useful because it relates modifications of the pulsation frequency directly to changes in the stellar model, *without needing* $\delta\xi$.

The next obvious question is what types of perturbations can we expect in stars? A first type of perturbation, which in fact is ubiquitous, is stellar rotation. One can distinguish the 1D case, where the rotation profile, Ω , only depends on the radial coordinate r (also known as ‘‘shellular’’ rotation) from the 2D case where it depends on r and θ , the colatitude. A second type of perturbation is modifications to the stellar structure, as defined, for instance, by the ρ_0 , $\Gamma_{1,0}$, c_0^2 etc., profiles. So far, structural modifications have only been envisaged in a 1D setting.

Rotation leads to two inertial accelerations: the centrifugal and the Coriolis acceleration. The former distorts the shape of the star but is a second order effect, so will be neglected. The latter intervenes in the oscillatory motions and leads to first order effects on the frequencies. To first order, Euler’s equation takes on the form:

$$\omega^2 \xi = 2\omega m \Omega \xi - 2i\omega \Omega \times \xi + \frac{\nabla p'}{\rho_0} - \frac{\rho' g_0}{\rho_0} + \nabla \phi', \quad (8)$$

where Ω is the rotation profile, and $\Omega = \Omega \mathbf{e}_z$. From this we deduce:

$$\delta\mathcal{F}(\xi) = 2\omega m \Omega \xi - 2i\omega \Omega \times \xi. \quad (9)$$

In the 1D case, the frequency shift is given by

$$\delta\omega_{n,\ell,m} = \omega_{n,\ell,m} - \omega_{n,\ell,0} = m \int_0^R K_\Omega^{n\ell}(r) \Omega(r) dr, \quad (10)$$

where

$$K_\Omega^{n\ell} = \frac{\rho_0 r^2 (\xi_r^2 + \ell(\ell+1)\xi_h^2 - 2\xi_r \xi_h - \xi_h^2)}{\int_0^R \rho_0(r) (\xi_r^2 + \ell(\ell+1)\xi_h^2) r^2 dr} \quad (11)$$

and where ξ_r and ξ_h are the radial and horizontal components of the Lagrangian displacement, respectively. $K_\Omega^{n\ell}$ is known as the ‘‘rotation kernel’’. As can be seen from this expression, frequencies with the same (n, ℓ) values are uniformly split as

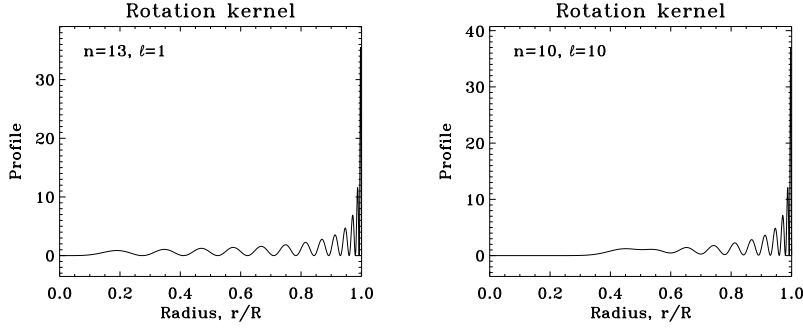


Fig. 1 Examples of 1D rotation kernels.

a function of m thanks to rotation. Figure 1 shows some examples of 1D rotation kernels.

If Ω is constant, then Eq. (10) simplifies to $\delta\omega = m(1 - \mathcal{C})\Omega$, where

$$\mathcal{C} = \frac{\int_0^R \rho_0 (2\xi_r \xi_h + \xi_h^2) r^2 dr}{\int_0^R \rho_0(r) (\xi_r^2 + \ell(\ell+1)\xi_h^2) r^2 dr}. \quad (12)$$

\mathcal{C} is known as the Ledoux constant and represents the effects of the Coriolis force (see Ledoux 1951).

In the 2D case, the rotational splitting is given by

$$\delta\omega_{n,\ell,m} = \int_0^R \int_0^\pi \mathcal{K}_{n,\ell,m}(r, \theta) \Omega(r, \theta) r dr d\theta, \quad (13)$$

where $\mathcal{K}_{n,\ell,m}(r, \theta)$ is the 2D rotation kernel (expressions for such kernels may be found in Schou et al. 1994). This time, the splitting as a function of m may be non-uniform.

The acoustic structure of stars is typically determined by two variables, e.g., $(\rho_0, \Gamma_{1,0})$ and possibly some surface quantities such as the surface pressure. Accordingly, when modifying the structure of a star, the modifications to two structural quantities need to be specified, e.g., $(\delta\rho_0, \delta\Gamma_{1,0})$ (although in some cases, 3 functions need to be specified, e.g., Buldgen et al. 2017). As was the case for rotation, it is possible to relate changes in frequency to structural modifications of stars using kernels. The easiest structural kernels to derive are those for the variables (ρ, c^2) . After a (very) lengthy derivation, one can show that

$$\frac{\delta\omega}{\omega} = \int_0^R \left[K_{c^2, \rho}(r) \frac{\delta c_0^2(r)}{c_0^2(r)} + K_{\rho, c^2}(r) \frac{\delta \rho_0(r)}{\rho_0(r)} \right] dr, \quad (14)$$

where:

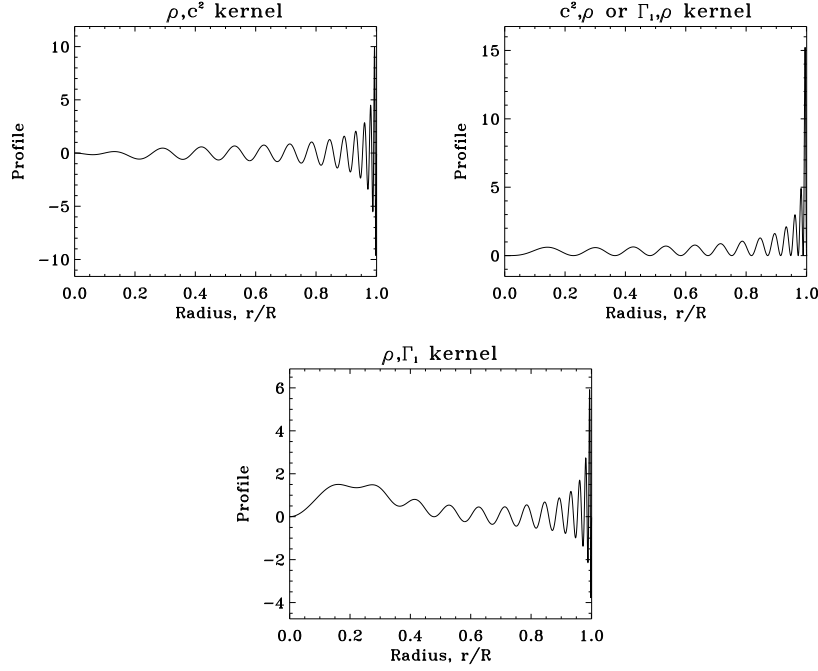


Fig. 2 Kernels for the $(n, \ell) = (13, 1)$ pulsation mode, for the structural pairs (ρ_0, c_0^2) and $(\rho_0, \Gamma_{1,0})$.

$$K_{c^2, \rho} = \frac{\rho_0 c_0^2 \chi^2 r^2}{2I\omega^2}, \quad (15)$$

$$K_{\rho, c^2} = \frac{\rho_0 r^2}{2I\omega^2} \left\{ c_0^2 \chi^2 - \omega^2 (\xi_r^2 + \ell(\ell+1)\xi_h^2) - 4\pi G \int_{s=r}^R \left(2\rho_0 \xi_r \chi + \frac{d\rho_0}{ds} \xi_r^2 \right) ds \right. \\ \left. - 2g_0 \xi_r \chi + 2g_0 \xi_r \frac{d\xi_r}{dr} + 4\pi G \rho_0 \xi_r^2 + 2 \left(\xi_r \frac{d\phi'}{dr} + \frac{\ell(\ell+1)\xi_h \phi'}{r} \right) \right\}, \quad (16)$$

$$I = \int_0^R \rho_0 (\xi_r^2 + \ell(\ell+1)\xi_h^2) r^2 dr, \quad \chi = \frac{\nabla \cdot \xi}{Y_m^\ell} = \frac{d\xi_r}{dr} + \frac{2\xi_r}{r} - \frac{\ell(\ell+1)\xi_h}{r}.$$

Figure 2 gives an example of (ρ, c^2) kernels. We note that in deriving Eq. (14), we neglected various surface terms which result from integration by parts. Also, the modelling of surface layers in stars tends to be inaccurate. Accordingly, Eq. (14) typically includes an extra ad hoc adjustable surface term.

Besides these kernels, other structural kernels can also be obtained: (ρ, Γ_1) , (P, Γ_1) , $(u \equiv \frac{p}{\rho}, \Gamma_1)$, (g, Γ_1) , (u, Y) , (A, Γ_1) , (N^2, c^2) etc. (see Masters 1979, Gough & Thompson 1991, Elliott 1996, Basu & Christensen-Dalsgaard 1997, Kosovichev 1999, Buldgen et al. 2017). Some of these require using the equation of state and its derivatives. Figure 2 shows an example of (ρ, Γ_1) kernels.

3 The inverse problem

As described at the beginning of this lecture, the seismic inverse problem consists in deducing the stellar structure from a set of *identified* pulsation frequencies, i.e., with known quantum numbers. Inverse methods have proved to be a powerful way of solving such a problem. These typically involve correcting a reference stellar model so as to obtain a new model which reproduces the pulsation frequencies more accurately. Inverse methods come into two broad categories, namely linear and non-linear methods. The linear methods are further subdivided into the Regularised Least-Squares (RLS) and Optimally Localised Averages (OLA) methods. For the non-linear inversions, there are iterated versions of the RLS method, as well as a method which adjusts the internal phases of the eigenmodes. In what follows, we will focus on linear inverse methods, beginning with rotation inversions, as these provide a good starting point to illustrate the different methods.

3.1 Rotation inversions

The rotation inverse problem can be expressed by the following set of equations:

$$S_{n_l, \ell_l} = \frac{\omega_{n_l, \ell_l, m_l} - \omega_{n_l, \ell_l, 0}}{m_l} = \int_0^R K_{\Omega}^{n_l, \ell_l}(r) \Omega(r) dr + \varepsilon_{n_l, \ell_l}, \quad 1 \leq l \leq L, \quad (17)$$

where the S_{n_l, ℓ_l} are the “rotational splittings” (i.e., the observations), $\Omega(r)$ the unknown rotation profile, and $\varepsilon_{n_l, \ell_l}$ the errors on the splittings, characterised by a standard deviation of $\sigma_{n_l, \ell_l} = \langle \varepsilon_{n_l, \ell_l} \rangle$. In what follows, we will use the index “ l ” as shorthand for (n_l, ℓ_l) .

The goal of the inverse problem is to recover $\Omega(r)$ from the set of available rotational splittings. At first, this problem looks impossible. Indeed, the unknown is a function, whereas there is a finite number of observational constraints. Furthermore, the problem is ill-conditioned, i.e., it is highly sensitive to noise. In order to address these issues, it is necessary to inject *a priori* assumptions when solving the inverse problem. Accordingly, we should always bear in mind these assumptions when looking at and interpreting the results.

3.1.1 Regularised Least Squares (RLS)

A first approach to tackling this problem involves decomposing the rotation profile over a set of basis functions:

$$\Omega_{\text{inv}}(r) = \sum_k a_k f_k(r), \quad (18)$$

where the a_k are unknown coefficients, and the f_k basis functions. In general, the number of unknown coefficients should be equal to or less than the number of observed splittings. Typical choices for the f_k include b-spline functions of various degrees. For instance, zeroth degree b-splines produce step-wise functions, whereas cubic splines produce functions with a continuous second derivative (which can be useful for regularisation terms).

When substituted into Eq. (17), this leads to the following theoretical rotational splittings, \tilde{S}_l , for the above rotation profile:

$$\tilde{S}_l = \int_0^R K_{\Omega}^l(r) \Omega_{\text{inv}}(r) dr. \quad (19)$$

An obvious way of choosing the a_k is by minimising (typically in a least-squares sense) the distance between the observed splittings, S_l , and the theoretical ones. However, a naive application of such a procedure leads to poor results as illustrated by the dotted grey curve in the top panel of Fig. 3. Indeed, the problem is ill-conditioned, and any errors in the observations will be strongly amplified.

A standard remedy to this problem is to include a supplementary regularisation term to obtain a smooth solution when carrying out the minimisation, hence the name ‘‘Regularised Least-Squares’’ (RLS) method. This leads to the following typical cost function:

$$J(a_k) = \sum_{l=1}^L \frac{(S_l - \tilde{S}_l)^2}{\sigma_l^2} + \Lambda \left\langle \frac{1}{\sigma^2} \right\rangle \int_0^R \left(\frac{d^2 \Omega_{\text{inv}}}{dr^2} \right)^2 dr, \quad (20)$$

where $\left\langle \frac{1}{\sigma^2} \right\rangle = \frac{1}{L} \sum_{l=1}^L \frac{1}{\sigma_l^2}$, and Λ is a regularisation parameter which can be adjusted. The cost function is minimised by numerically finding the a_k coefficients for which the gradient of J is zero.

Figure 3 shows various solutions obtained for the rotation inverse problem based on a set of rotational splittings from Christensen-Dalsgaard et al. (1990). As can be seen in the top panel, larger values of Λ lead to solutions that are smoother. The bottom panel shows that such solutions are a worse fit to the S_l . Hence, there is a trade-off between obtaining smooth solutions and fitting the data. The best solutions are obtained for intermediate values of Λ as can be seen by comparing the solutions in Fig. 3 to the true solution given in figs. 3 and 11 of Christensen-Dalsgaard et al. (1990).

3.1.2 Various error measurements

It is also possible to calculate error bars around the inverted solution. To demonstrate this, we start with a given grid point, r_0 . The relationship between $\Omega_{\text{inv}}(r_0)$ and the a_k coefficients is linear. Likewise, the relationship between the a_k and the S_l is also linear. Hence the relationship between $\Omega_{\text{inv}}(r_0)$ and the S_l is linear and can be expressed as follows:

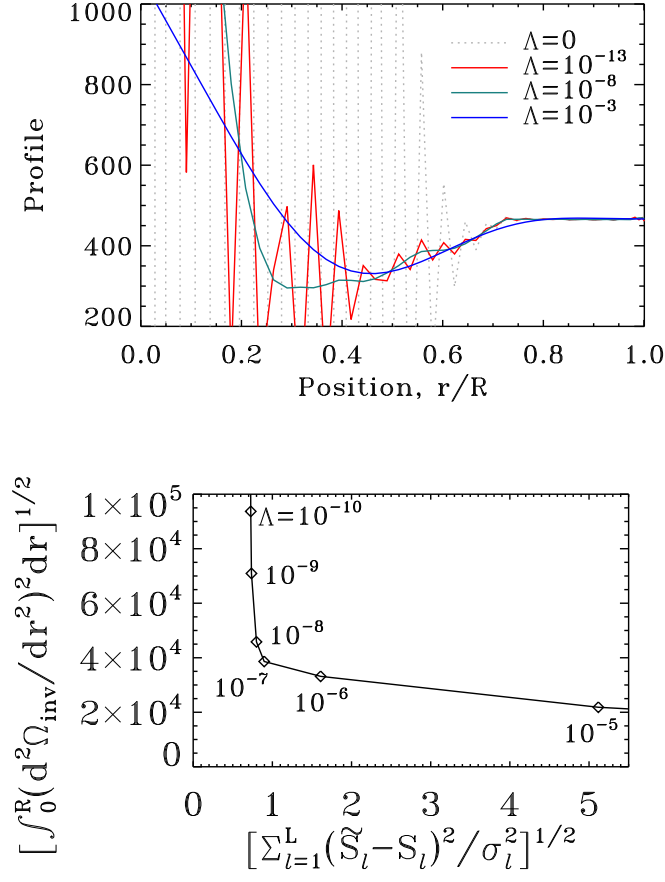


Fig. 3 *Top:* Inverted rotation profiles based on the RLS method for different values of the regularisation parameter. *Bottom:* L-curve which shows the two components of the RLS cost function as a function of Λ .

$$\Omega_{\text{inv}}(r_0) = \sum_l c_l(r_0) S_l. \quad (21)$$

Assuming the errors on the splittings are uncorrelated, the 1σ error bar on the inverted value of the rotation rate will simply be

$$\sigma_{\Omega(r_0)} = \sqrt{\sum_l (c_l(r_0) \sigma_l)^2}. \quad (22)$$

In the specific case where the errors are uniform, the error is amplified by the quantity $\sqrt{\sum_l (c_l(r_0))^2}$ which is known as the ‘‘error magnification’’. It is important to

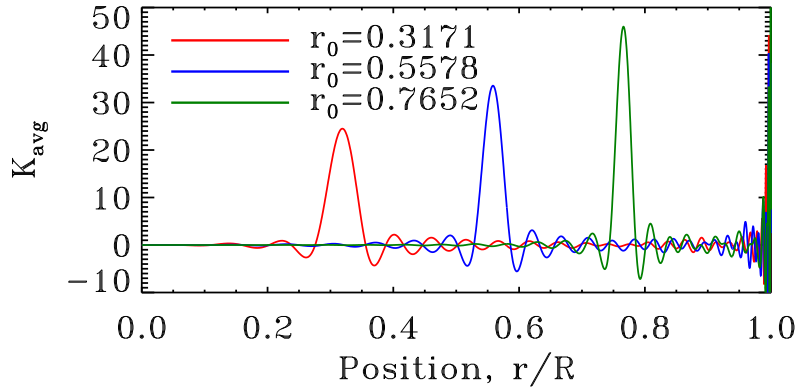


Fig. 4 Averaging kernels for the RLS method at various positions.

bear in mind that these error bars only take into account how the observational errors propagate through the inversion. They do not actually measure the quality of the inversion, which could, for example, be poor due to over-regularisation.

In order to evaluate the quality of the inversion at a given point, it is useful to look at the “averaging kernel”. If we replace the S_l in Eq. (21) by the expressions given in Eq. (17), then it is possible to establish a relationship between $\Omega(r)$ and $\Omega_{\text{inv}}(r_0)$:

$$\Omega_{\text{inv}}(r_0) = \int_0^R \underbrace{\sum_l c_l(r_0) K_{\Omega}^l(r)}_{\mathcal{K}_{\text{avg}}(r_0, r)} \Omega(r) dr + \sum_l c_l(r_0) \varepsilon_l. \quad (23)$$

This expression shows that $\Omega_{\text{inv}}(r_0)$ is in fact an average of the true rotation profile $\Omega(r)$. The corresponding weight function, $\mathcal{K}_{\text{avg}}(r_0, r)$, is the averaging kernel. Ideally, this function should have a strong amplitude at r_0 and be close to zero elsewhere. Figure 4 shows a few examples of averaging kernels for the RLS method.

3.1.3 Optimally Localised Averages (OLA)

The notion of averaging kernels naturally leads to the Optimally Localised Averages (OLA) methods. The basic idea in these methods is to optimise the coefficients c_l so as to obtain *optimal* averaging kernels. Two variants include the Multiplicative and the Subtractive OLA, abbreviated MOLA and SOLA, respectively.

The MOLA method comes from Backus & Gilbert (1968). In this method, the averaging kernel is *multiplied* by a penalty function that increases in amplitude as you move away from the target position r_0 . Hence, the coefficients $c_l(r_0)$ are obtained by minimising the following cost function:

$$J(c_l) = \underbrace{\int_0^R P(r_0, r) [\mathcal{K}_{\text{avg}}(r_0, r)]^2 dr}_{\text{fit data}} + \underbrace{\frac{\tan \theta}{\langle \sigma^2 \rangle} \sum_{l=1}^L (c_l \sigma_l)^2}_{\text{regularisation}} + \lambda \underbrace{\left\{ 1 - \int_0^R \mathcal{K}_{\text{avg}} \right\}}_{\mathcal{K}_{\text{avg}} \text{ unimodular}}, \quad (24)$$

where $\langle \sigma^2 \rangle = \frac{1}{L} \sum_{l=1}^L \sigma_l^2$, θ is a trade-off parameter between fitting data and reducing error (i.e., a regularisation parameter), $P(r_0, r)$ the penalty function (usually $12(r - r_0)^2$), and λ a Lagrange multiplier used to ensure that the averaging kernel is “unimodular”, i.e., $\int_0^R \mathcal{K}_{\text{avg}}(r_0, r) dr = 1$. This last condition is important for ensuring that the inverted value, $\Omega_{\text{inv}}(r_0) = \sum_l c_l(r_0) S_l$ is a proper average of the underlying rotation profile.

The SOLA method was first described in Pijpers & Thompson (1992). In this method, the *difference* between the averaging kernel and a suitable target function is minimised. Hence, the coefficients $c_l(r_0)$ are obtained by minimising the following cost function:

$$J(c_l) = \int_0^R [\mathcal{T}(r_0, r) - \mathcal{K}_{\text{avg}}(r_0, r)]^2 dr + \frac{\tan \theta}{\langle \sigma^2 \rangle} \sum_{l=1}^L (c_l \sigma_l)^2 + \lambda \left\{ 1 - \int_0^R \mathcal{K}_{\text{avg}} \right\}, \quad (25)$$

where $\mathcal{T}(r_0, r)$ is the target function. Ideally, \mathcal{T} should be a Dirac function centred on r_0 . However, given the finite number of rotation splittings and hence rotation kernels to work with, trying to achieve such a target is impossible and would lead to poor numerical results. Generally, Gaussian or similar functions are used as targets:

$$\mathcal{T}(r_0, r) = \frac{1}{A} \exp\left(-\frac{(r - r_0)^2}{2\Delta(r_0)^2}\right), \quad (26)$$

where A is a normalisation constant to ensure that $\int_0^R \mathcal{T}(r_0, r) dr = 1$ (it is not simply $1/\sqrt{2\pi}\Delta(r_0)$ since the integration interval is not from $-\infty$ to ∞), and $\Delta(r_0)$ the width of the target function. A good choice for $\Delta(r_0)$ when dealing with acoustic modes is $\Delta(r_0) \propto c_0(r_0)$ (e.g., Thompson 1993).

Figure 5 shows inversion results for the RLS, MOLA and SOLA methods as well as some averaging kernels. The advantages of the MOLA method compared to the SOLA method is that it has fewer free parameters and tends to produce slightly better results. Conversely, the SOLA method has a much smaller computational cost. Indeed, minimising the SOLA cost function for different values of r_0 leads to systems of equations where only the right-hand side changes. Accordingly, only one matrix inversion (or factorisation) is needed for the entire inversion.

3.1.4 Applications

The first and most spectacular examples of rotation profile inversions are those done for the Sun. Indeed, the Sun’s close proximity has enabled the detection of countless rotational splittings going to high ℓ values. This, in turn, has enabled 2D in-

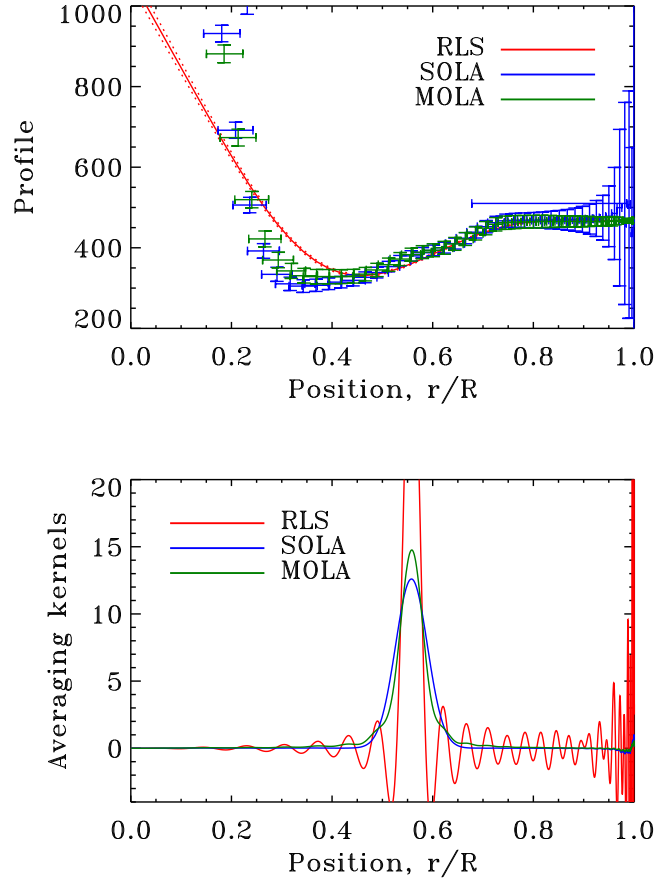


Fig. 5 *Top*: Inversion results and error bars for the RLS, MOLA and SOLA methods. *Bottom*: Averaging kernels at $r_0 = 0.5578R$ for these three methods.

versions of the solar rotation profile such as the one shown in Fig. 6, taken from Thompson et al. (2003) (see also Schou et al. 1998). Such profiles were not in agreement with the theoretical predictions at the time and have accordingly led to various theoretical investigations and numerical simulations to gain a better understanding of the Sun and its internal rotation (e.g., Thompson et al. 2003, Brun et al. 2004).

A more recent example of stellar rotation inversions are those in subgiants and red giants (Deheuvels et al. 2012, 2014). These results as well as results from ensemble asteroseismology have shown that although the core of these stars rotate much faster than the envelope, the difference in rotation speeds is orders of magnitude smaller than what is expected theoretically (Eggenberger et al. 2012,

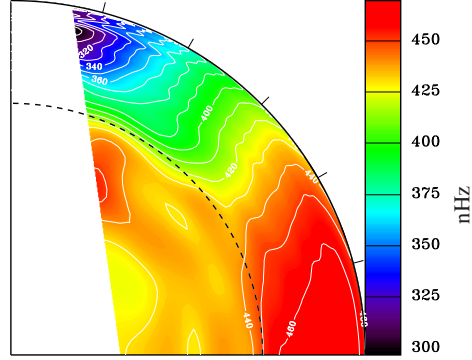


Fig. 6 2D solar rotation profile from Thompson et al. (2003) (see also Schou et al. 1998) based on a SOLA inversion technique. Figure courtesy of M. J. Thompson and J. Christensen-Dalsgaard.

Ceillier et al. 2013, Marques et al. 2013). It is still an open question what transport mechanisms are involved in these stars and could solve this discrepancy.

3.2 Structural inversions

We now turn our attention to structural inversions. In contrast to rotation inversions, there are *two* functions to invert simultaneously. As was derived in Sect. 2.3, the linearised relationship between modifications of the stellar structure and shifts in the frequency can be expressed as follows:

$$\underbrace{\frac{\delta \omega_l}{\omega_l}}_{\text{obs.}} = \int_0^R \underbrace{K_{a,b}^l(r)}_{\text{known}} \underbrace{\frac{\delta a}{a}}_{\text{unknown}} dr + \int_0^R \underbrace{K_{b,a}^l(r)}_{\text{known}} \underbrace{\frac{\delta b}{b}}_{\text{unknown}} dr + \frac{F_{\text{surf.}}(\omega_l)}{E_l} + \varepsilon_l, \quad (27)$$

where we have added an ad hoc surface correction term (i.e., the term with $F_{\text{surf.}}$) as well as the observational error, ε_l . The variables (a, b) represent two structural profiles (e.g., (ρ, I_1)). The structural inverse problem then consists in deducing the profiles $\delta a/a$ and $\delta b/b$ from the frequency shifts $\delta \omega_l/\omega_l$. The fact that there are two functions to invert leads to modifications of the RLS and OLA methods, as well as the introduction of “cross-term kernels”, $\mathcal{K}_{\text{cross}}$.

3.2.1 Regularised Least Squares (RLS)

In the regularised least squares method, both functions ($\delta a/a$ and $\delta b/b$) are discretised over a set of basis functions, and the unknown coefficients are obtained by minimising a cost function of the form:

$$J\left(\frac{\delta a}{a}, \frac{\delta b}{b}\right) = \sum_l \frac{1}{\sigma_l^2} \left(\frac{\delta \omega_l}{\omega_l} - \int_0^R K_{a,b}^l \frac{\delta a}{a} dr - \int_0^R K_{b,a}^l \frac{\delta b}{b} dr \right)^2 + \Lambda \left\langle \frac{1}{\sigma^2} \right\rangle \int_0^R \left[\left(\frac{d^2 \delta a}{dr^2} \frac{1}{a} \right)^2 + \left(\frac{d^2 \delta b}{dr^2} \frac{1}{b} \right)^2 \right] dr. \quad (28)$$

Additional terms may be included to model surface effects.

In much the same way as for rotation inversions, the inverted functions are related in a linear way to the observables $(\delta \omega / \omega)_l$:

$$\left(\frac{\delta a}{a} \right)_{\text{inv}} = \sum_l c_l(r_0) \left(\frac{\delta \omega}{\omega} \right)_l, \quad \left(\frac{\delta b}{b} \right)_{\text{inv}} = \sum_l c'_l(r_0) \left(\frac{\delta \omega}{\omega} \right)_l. \quad (29)$$

These inversion coefficients can then be used to define the averaging and cross-term kernels:

$$\mathcal{H}_{\text{avg}}(r_0, r) = \sum_{l=1}^L c_l(r_0) K_{a,b}^l(r), \quad \mathcal{H}_{\text{cross}}(r_0, r) = \sum_{l=1}^L c_l(r_0) K_{b,a}^l(r), \quad (30)$$

$$\mathcal{H}'_{\text{avg}}(r_0, r) = \sum_{l=1}^L c'_l(r_0) K_{b,a}^l(r), \quad \mathcal{H}'_{\text{cross}}(r_0, r) = \sum_{l=1}^L c'_l(r_0) K_{a,b}^l(r), \quad (31)$$

which help to relate the inverted structural functions at r_0 to the true structural functions:

$$\left(\frac{\delta a}{a} \right)_{\text{inv}}(r_0) = \int_0^R \left[\mathcal{H}_{\text{avg}}(r_0, r) \frac{\delta a(r)}{a(r)} + \mathcal{H}_{\text{cross}}(r_0, r) \frac{\delta b(r)}{b(r)} \right] dr, \quad (32)$$

$$\left(\frac{\delta b}{b} \right)_{\text{inv}}(r_0) = \int_0^R \left[\mathcal{H}'_{\text{cross}}(r_0, r) \frac{\delta a(r)}{a(r)} + \mathcal{H}'_{\text{avg}}(r_0, r) \frac{\delta b(r)}{b(r)} \right] dr, \quad (33)$$

where we have neglected the contribution from surface effects and observational errors. As can be seen from these equations, the cross-term kernels help to quantify the amount of cross-talk between the two functions in the inversion.

In the particular case of solar inversions, where the mass is known through independent considerations, it is possible to constrain the inversion to preserve the mass by introducing a supplementary Lagrange multiplier, provided one of the structural variables being inverted is the density variation, $\delta \rho_0 / \rho_0$. Indeed, if the mass is constant, then $\delta \rho_0 / \rho_0$ obeys the following relation:

$$0 = 4\pi \int_0^R \rho_0(r) \frac{\delta \rho_0}{\rho_0} r^2 dr. \quad (34)$$

3.2.2 Optimally Localised Averages (OLA)

The OLA methods will also be modified due to the presence of two functions which are being inverted. Given that the modifications to the MOLA and SOLA variants are similar, we will focus on the SOLA method in what follows. First of all, there will be two separate inversions, one for each of the functions being inverted. Secondly, not only do the averaging kernels need to be optimised, but the cross-term kernels need to be reduced as much as possible. These considerations lead to cost functions of the following form:

$$J(c_l(r_0)) = \int_0^R \{ \mathcal{T}(r_0, r) - \mathcal{K}_{\text{avg}}(r_0, r) \}^2 dr + \beta \int_0^R \{ \mathcal{K}_{\text{cross}}(r_0, r) \}^2 dr + \frac{\tan \theta \sum_{l=1}^L (c_l(r_0) \sigma_l)^2}{\langle \sigma^2 \rangle} + \lambda \left\{ 1 - \int_0^R \mathcal{K}_{\text{avg}}(r_0, r) dr \right\}. \quad (35)$$

For each inversion, there is a regularisation parameter (θ), a supplementary parameter to adjust the trade-off between optimising the averaging kernel or minimising the cross-term kernel (β), a Lagrange multiplier to ensure the averaging kernel is unimodular (λ), and optionally some supplementary Lagrange multipliers used to suppress surface effects (Däppen et al. 1991). The target functions (\mathcal{T}) for each of the inverted functions can be adjusted independently.

In order to preserve the mass, for instance in the case of solar inversions, one can treat Eq. (34) as a supplementary observed relation. Specifically, 0 will play the role of $\delta\omega/\omega$ and the function $f(r) = 4\pi\rho r^2$ will be the kernel associated with the structural variable $\delta\rho_0/\rho_0$.

3.2.3 Applications

Up to now, structural inversions have been applied primarily to the Sun. Figure 7, which is based on the results of Basu et al. (2009), shows an example of such an inversion for the structural variables (c, ρ). In recent years, the downward revision of the solar metal abundances (e.g., Asplund et al. 2009) has led to a significant discrepancy between the results from solar structural inversions and models based on these new abundances (e.g., Basu et al. 2015). Indeed, helioseismic inversions led to a lower depth for the base of the convection zone compared to what is obtained from models with the revised abundances. Currently, it is not entirely clear how to solve this problem but different solutions are being investigated.

3.3 Integrated quantities

In the case of stars other than the Sun, it is very difficult to carry out structural inversions due to the limited number of available modes (e.g., Basu et al. 2002).

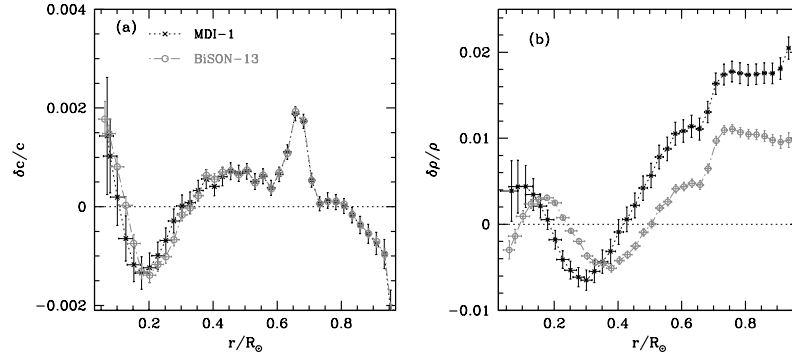


Fig. 7 (c, ρ) structural inversion for the Sun based on the results of Basu et al. (2009). Figure courtesy of S. Basu.

Indeed, because of cancellation effects in disc-integrated observations, only modes for which $\ell \leq 3$ are detected (Dziembowski 1977). One strategy in such a situation is to invert stellar parameters rather than structural profiles. Indeed, since structural inversions at a given grid point actually give a weighted average of the true underlying profile, one can use a SOLA inversion to directly target the appropriate weight function which yields the desired stellar parameter. The quantities which may be inverted by such a procedure include the total angular momentum (Pijpers 1998), the mean density (Reese et al. 2012), the acoustic radius and various core or internal mixing indicators (Buldgen et al. 2015b,a, 2017). Figure 8 shows an inversion of the acoustic radius, as described in Buldgen et al. (2015b).

4 Conclusion

As illustrated in this course, inversions can be used to probe stellar rotation profiles, probe the internal structure of stars, estimate various stellar parameters, and indirectly test new physics outside a given grid of stellar models. Nonetheless, one must also bear the limitations of seismic inversions, namely, the use of a priori assumptions about the smoothness of rotation or structural profiles and the linearisation of the relationship between frequencies and stellar structure (except in the case of non-linear inversions). Furthermore, it is important to keep in mind that inversions cannot yield more information than what is intrinsically contained in the observed pulsation modes.

In order to get a more in-depth understanding of inversions, we recommend the following articles or publications:

- Lynden-Bell & Ostriker (1967) and Christensen-Dalsgaard (2003): the variational principle
- Gough & Thompson (1991): structural kernels

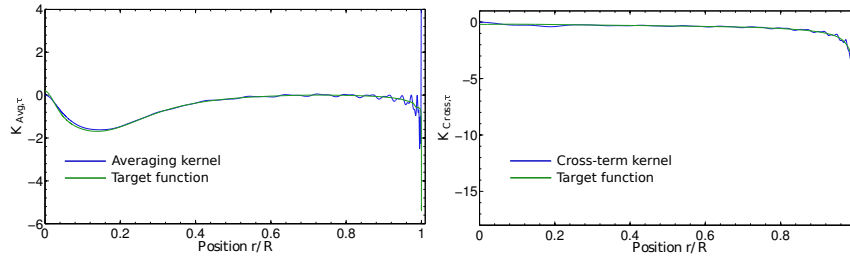


Fig. 8 Acoustic radius inversion based on Buldgen et al. (2015b). Figure courtesy of G. Buldgen.

- Christensen-Dalsgaard et al. (1990): error propagation and magnification, averaging kernels
- Rabello-Soares et al. (1999): adjusting the free parameters in inversions
- Reese et al. (2012) and Buldgen et al. (2015b): inversions of integrated quantities

We also note that the recent monograph by Pijpers (2006) contains several chapters on helioseismic and asteroseismic inversions.

Various seismic inversion software packages have also become freely available in recent years:

- INVERSIONKIT⁴: 1D inversions on individual stars
- INVERSIONPIPELINE⁵: inversions of stellar parameters using a grid of models
- NONLINEARKIT⁶: non-linear 1D inversion tool still under development
- SOLA PACK⁷: 2D rotation inversions in the Sun

Acknowledgements I would like to thank the organisers of this Summer School for giving me the opportunity to give this lecture on inversions. Furthermore, I thank M. J. Thompson for introducing me to inversions, as well as S. Basu and G. Buldgen for many discussions on the topic.

References

- Asplund, M., Grevesse, N., Sauval, A. J., & Scott, P. 2009, *ARA&A*, 47, 481
 Backus, G., & Gilbert, F. 1968, *Geophysical Journal*, 16, 169
 Basu, S., Chaplin, W. J., Elsworth, Y., New, R., & Serenelli, A. M. 2009, *ApJ*, 699, 1403
 Basu, S., & Christensen-Dalsgaard, J. 1997, *A&A*, 322, L5
 Basu, S., Christensen-Dalsgaard, J., & Thompson, M. J. 2002, in *ESA Special Publication*, Vol. 485, *Stellar Structure and Habitable Planet Finding*, ed. B. Battrock, F. Favata, I. W. Roxburgh, & D. Galadi, 249–252

⁴ See <http://bison.ph.bham.ac.uk/spaceinn/inversionkit>.

⁵ See <http://bison.ph.bham.ac.uk/spaceinn/inversionpipeline>.

⁶ See <http://bison.ph.bham.ac.uk/spaceinn/nonlinearkit>.

⁷ See <http://sun.stanford.edu/~rmunk/SOLAPack/index.html>.

- Basu, S., Grevesse, N., Mathis, S., & Turck-Chièze, S. 2015, *Space Science Reviews*, 196, 49
- Bazot, M., Bourguignon, S., & Christensen-Dalsgaard, J. 2012, *MNRAS*, 427, 1847
- Brun, A. S., Miesch, M. S., & Toomre, J. 2004, *ApJ*, 614, 1073
- Buldgen, G., Reese, D. R., & Dupret, M. A. 2015a, *A&A*, 583, A62
- . 2017, *A&A*, 598, A21
- Buldgen, G., Reese, D. R., Dupret, M. A., & Samadi, R. 2015b, *A&A*, 574, A42
- Ceillier, T., Eggenberger, P., García, R. A., & Mathis, S. 2013, *A&A*, 555, A54
- Charpinet, S., Fontaine, G., Brassard, P., Green, E. M., & Chayer, P. 2005, *A&A*, 437, 575
- Christensen-Dalsgaard, J. 2003, *Lecture Notes on Stellar Oscillations*, <http://astro.phys.au.dk/~jcd/oscilnotes/>
- . 2008, *ApSS*, 316, 113
- Christensen-Dalsgaard, J., Schou, J., & Thompson, M. J. 1990, *MNRAS*, 242, 353
- Däppen, W., Gough, D. O., Kosovichev, A. G., & Thompson, M. J. 1991, in *Lecture Notes in Physics*, Berlin Springer Verlag, Vol. 388, *Challenges to Theories of the Structure of Moderate-Mass Stars*, ed. D. Gough & J. Toomre, 111
- Deheuvels, S., García, R. A., Chaplin, W. J., et al. 2012, *ApJ*, 756, 19
- Deheuvels, S., Doğan, G., Goupil, M. J., et al. 2014, *A&A*, 564, A27
- Dziembowski, W. 1977, *Acta Astronomica*, 27, 203
- Eggenberger, P., Montalbán, J., & Miglio, A. 2012, *A&A*, 544, L4
- Elliott, J. R. 1996, *MNRAS*, 280, 1244
- Gough, D. 1985, *Sol. Phys.*, 100, 65
- Gough, D. O., & Thompson, M. J. 1991, in *Solar Interior and Atmosphere*, ed. Cox, A. N., Livingston, W. C., & Matthews, M. S. (University of Arizona Press, Tucson), 519–561
- Kosovichev, A. G. 1999, *Journal of Computational and Applied Mathematics*, 109, 1
- Ledoux, P. 1951, *ApJ*, 114, 373
- Lynden-Bell, D., & Ostriker, J. P. 1967, *MNRAS*, 136, 293
- Marques, J. P., Goupil, M. J., Lebreton, Y., et al. 2013, *A&A*, 549, A74
- Masters, G. 1979, *Geophysical Journal*, 57, 507
- Metcalfe, T. S., & Charbonneau, P. 2003, *Journal of Computational Physics*, 185, 176
- Pijpers, F. P. 1998, *MNRAS*, 297, L76
- . 2006, *Methods in helio- and asteroseismology* (Imperial College Press)
- Pijpers, F. P., & Thompson, M. J. 1992, *A&A*, 262, L33
- Rabello-Soares, M. C., Basu, S., & Christensen-Dalsgaard, J. 1999, *MNRAS*, 309, 35
- Reese, D. 2006, PhD thesis, Université Toulouse III - Paul Sabatier, <http://tel.archives-ouvertes.fr/tel-00120334>
- Reese, D. R., Marques, J. P., Goupil, M. J., Thompson, M. J., & Deheuvels, S. 2012, *A&A*, 539, A63
- Schou, J., Christensen-Dalsgaard, J., & Thompson, M. J. 1994, *ApJ*, 433, 389
- Schou, J., Antia, H. M., Basu, S., et al. 1998, *ApJ*, 505, 390

- Silva Aguirre, V., Davies, G. R., Basu, S., et al. 2015, *MNRAS*, 452, 2127
- Thompson, M. J. 1993, in *Astronomical Society of the Pacific Conference Series*, Vol. 42, GONG 1992. Seismic Investigation of the Sun and Stars, ed. T. M. Brown, 141
- Thompson, M. J., Christensen-Dalsgaard, J., Miesch, M. S., & Toomre, J. 2003, *ARA&A*, 41, 599
- Unno, W., Osaki, Y., Ando, H., Saio, H., & Shibahashi, H. 1989, *Nonradial oscillations of stars* (Tokyo: University of Tokyo Press)